Feasibility of Detecting Hypoxia in Experimental Mouse Tumours with ^{18}F-fluorinated Tracers and Positron Emission Tomography

A Study Evaluating [^{18}F]Fluoromisonidazole and [^{18}F]Fluoro-2-deoxy-D-glucose

Lise Bentzen, Susanne Keiding, Michael R. Horsman, Lise Falborg, Søren B. Hansen and Jens Overgaard

From the Danish Cancer Society, Department of Experimental Clinical Oncology (L. Bentzen, M.R. Horsman, J. Overgaard), the PET Centre (S. Keiding, L. Falborg, S. B. Hansen) and the Department of Medicine V (S. Keiding), Aarhus University Hospital, Aarhus, Denmark

Correspondence to: Dr Lise Bentzen, Department of Experimental Clinical Oncology, Aarhus University Hospital, Nørrebrogade 44, Build. 5, DK-8000 Aarhus C, Denmark. Tel: + 45 89 49 26 20. Fax: + 45 86 19 71 09. E-mail: Lise@oncology.dk

Acta Oncologica Vol. 39, No. 5, pp. 629–637, 2000

The study was designed to investigate the binding of [^{18}F]Fluoromisonidazole ([^{18}F]FMISO) and [^{18}F]Fluoro-2-deoxy-D-glucose ([^{18}F]FDG) in a C3H mouse mammary carcinoma. Non-anaesthetized tumour-bearing animals breathing either normal air or carbogen (to reduce tumour hypoxia) were examined by PET after tracer injection. Tumours were identified by radioactive labelling and methods of defining regions of interest (ROI) in the tumours were investigated. Reference tissue was selected elsewhere in the mice and the ratio between mean radioactivity in tumour and reference tissue was compared. The results showed a correlation between the methods of identifying ROIs and a significantly lower tumour to reference tissue ratio for carbogen-treated mice compared with controls when using [^{18}F]FMISO. Only one of the methods showed a significant difference in the tumour labelling between treatment groups using [^{18}F]FDG. The study supports the contention that [^{18}F]FMISO may be able to identify hypoxia in tumours, whereas a similar role for [^{18}F]FDG is more doubtful.

Received 19 October 1999
Accepted 15 March 2000

It has been shown that hypoxic cells in some solid tumours contribute to cancer therapy resistance (1–4). More recent studies have provided evidence that hypoxia may also contribute to malignant progression through its effects on signal transduction pathways and the regulation of transcription of various genes. In particular, hypoxia can induce factors associated with apoptosis and angiogenesis, both of which will have profound effects on tumour growth and dissemination (5–8). Modifying hypoxia therefore has a central role in optimizing non-surgical cancer treatment. In spite of our knowledge about the importance of hypoxia on tumour progression and treatment outcome, the ability to identify and quantify tumour hypoxia in patients is still limited. Several methods for evaluating tumour hypoxia, both invasively and non-invasively, have been examined. At present, an invasive technique using oxygen sensitive electrodes measuring oxygen partial pressure (pO_2) distributions in the tumour tissue has shown a prognostic relationship with the extent of hypoxia (9–12). Attempts are now being made to develop non-invasive methods by means of physiological imaging techniques, such as magnetic resonance imaging (MRI), single photon emission computerized tomography (SPECT) and positron emission tomography (PET), for a review, see (13). With PET, positron-emitting labelled tracers are injected and radioactivity visualized by advanced imaging techniques, thus allowing for metabolic processes to be quantified. This includes the possibility of identifying the hypoxia marker fluoromisonidazole, bound in solid tumours.

Nitroimidazole compounds, like misonidazole and fluoromisonidazole, are reduced under hypoxic conditions and irreversibly bound to cellular macromolecules (14, 15). Labelling this compound with the positron emitter ^{18}F enables detection of the bound product by PET. Preliminary clinical studies have already reported that binding of this tracer can be detected in human tumours, but whether

 ISSN 0284-186X

this truly estimates hypoxia has not been established (13, 16, 17). The most commonly used tracer for PET examinations in oncology is the glucose analogue [^{18}F]Fluoro-2-deoxy-D-glucose ([^{18}F]FDG) which has been used for identification of tumours. Studies have suggested that FDG, which is phosphorylated in the cells but not further metabolized, should be accumulated in hypoxic cancer cells compared to normoxic cancer cells because of a changed metabolism (18, 19). However in vivo experiments have never shown a direct correlation between the uptake of FDG and the existence of hypoxia in tumours.

The aim of this work was to establish an experimental model where mice bearing tumours known to contain hypoxic cells could be examined by PET scanning using the radiolabelled tracer [^{18}F]Fluoromisonidazole ([^{18}F]FMISO). The aim was to measure the uptake of the tracer in the tumours and to define suitable methods to analyse and report the PET data for these experimental tumours. A further aim of the study was to examine whether the PET method could discriminate between different levels of tumour hypoxia when the tumour-bearing animals were exposed to gas breathing. Finally, we examined the radiolabelled tracer [^{18}F]FDG to clarify whether binding of this compound discriminated between different levels of hypoxia in our tumour model.

MATERIAL AND METHODS

Radiolabelled tracer

Fluoromisonidazole (FMISO) was produced by the nucleophilic fluorination of 1-(2′-nitro-1′-imidazolyl)-2-*O*-tetrahydropyranyl-3-*O*-toluenesulfonylpropandiole followed by acidic hydrolysis of the protecting group, as described by Lim & Berridge (20). The synthetic procedure was modified as follows: the synthesis of [^{18}F]FMISO was performed using the same equipment as that used for the synthesis of FDG (FDG Microlab, GE Medical Systems) (21). [^{18}F]Fluoride was produced by the ^{18}O(p,n)^{18}F nuclear reaction using a GE Medical Systems PETtrace 17 MeV cyclotron for bombardment of 1200 µl ^{18}O enriched water with high-energy protons. The [^{18}F]fluoride was transferred, in a narrow bore teflon capillary, from the cyclotron to an automated FDG synthesis module situated in a dedicated lead shielded area in the radiochemistry laboratory. The four glass vials attached to the FDG kit were filled with the following chemicals: 1) 5 mg precursor (1-(2′-nitro-1′-imidazolyl)-2-*O*-tetrahydropyranyl-3-*O*-toluenesulfonylpropandiole, ABX advanced biochemical compounds); 2) 4 ml anhydrous acetonitrile; 3) 1 ml sterile Na_2HPO_4 buffer (made from 3.2 g $Na_2HPO_4 \cdot 2H_2O$ and 536 mg NaOH in 100 ml sterile water) and 2 ml sterile water; 4) 2 ml 0.1 M sterile HCl solution. At the end of synthesis, the product was transferred to a hot cell for purification. The solution was automatically injected onto an HPLC system (column: phenominex, Nucleosil 5 C18, 250 × 10 mm; eluent: 5% EtOH solution; flow: 3.5 ml/min; detection: UV (320 nm) and radiodetection). The fraction containing [^{18}F]FMISO eluted after approximately 13 min and was collected, passed through a sterile filter and transferred to a sterile vial. Hypertonic saline was added to obtain an isotonic solution of the final product, containing about 500 MBq in 5 ml solution with a radiochemical purity of 100%. [^{18}F]FDG was synthesized at the PET centre by standard procedure (21).

Animals and tumours

Female mice CDF1 (12–16 weeks of age), weighing between 22 and 30 g, with a C3H mammary carcinoma grown on the backs were used. Derivation and maintenance have been described previously (22). This tumour has a known radiobiological hypoxic fraction, as calculated with the clamped tumour control assay, of 10–20% depending on size (23, 24). Tumour volumes were determined before the PET scanning by measuring the three orthogonal diameters D1, D2 and D3 and the volume was calculated as $\pi/6 \times D1 \times D2 \times D3$.

Experimental set-up and PET examination

The mice were kept anaesthetized during the preparation with 0.3 ml mebumal (4.76 mg/ml saline) injected intraperitoneally. The mice were not given any food for at least 3 h before the injection of tracer and the PET examination. A venflon catheter (0.8 mm/22G, length 25 mm) was used as a bladder catheter, with polythene tubing (outer diameter 0.38 mm, inner diameter 0.30 mm) connecting the catheter with a syringe used to flush saline through the bladder catheter. The animals were restrained in lucite plastic jigs and the tails of the animals were secured with tape to allow an intravenous (i.v.) line to be inserted into the tail vein. These i.v. lines consisted of butterfly needles (25G) and polythene tubing connecting the lines with the syringes containing the tracer. I.v.lines were flushed with heparine (100 IE/ml saline). The volume of the heparine solution was measured and adjusted for in the tracer injection and the volume of the tracer solution injected was kept low, 160 µl, in order to minimize changes in the plasma volume and circulation of the animals. The tracer was injected into the animals using a syringe infusion pump (22, Havard Apparatus, Southnatick, MA.). Injections were started at the beginning of the scanning procedure at a rate of 100 µl/min. The [^{18}F]FMISO dose was 925 kBq–3.20 MBq/animal with a median dose of 1.06 MBq. The [^{18}F]FDG dose was 1.05–1.25 MBq/animal. Six mice in their individual jigs were placed in a custom built, plastic device with the tumours located in a circle so that the distance from the tumours to the centre of the PET gantry was approximately the same (see Fig. 1 for a transaxial PET image). The animals were no longer anaesthetized when the scanning procedure was started.

Mice were positioned in the 60 cm opening of the Siemens ECAT EXACT HR (961) scanner, with the whole of each animal within the 15 cm field of view. Scanning was performed with 47 transaxial slices each of 3.1 mm in the 15 cm field of view, yielding radioactivity concentration measurements in voxels of $3.1 \times 2.4 \times 2.4$ mm^3. The scanning procedure started with a 15-min transmission scan, acquired before the injection of tracer and used for attenuation correction, followed by a dynamic PET scan of the animals lasting for a total of 5 h. The time-frame structure varied throughout both the individual examination and the study. Some data were recorded in 10-min time frames for the first 90 min and thereafter in 30-min time frames. However, typically experiments were carried out with 10-min frames throughout the whole measuring period. Data were reconstructed using a Ramp filter with a cut-off frequency of 0.5, resulting in an almost uniform resolution with a full width at half maximum (FWHM) of 4.5 mm. Data were recorded as integrated mean values of the radioactivity in each of the time frames and decay corrected to the start of the tracer injection.

During the PET examination, the bladders were flushed with saline at 60, 90, 120, 180 and 240 min after injection to minimize hot spots and spillover effects from the bladder on the tumour measurements. The rectal temperatures of the animals were measured after the examination to ensure that the animals' body temperature did not fall during the experiment.

Modification of hypoxia in the tumours

The animals were breathing either normal air, delivered through a custom-built nozzle placed in the front of the jig, or carbogen (95% oxygen and 5% carbon dioxide) gas at a flow rate of 2.5 l/min (2). The gassing procedure was started at least 5 min prior to the injection and continued throughout the experiment.

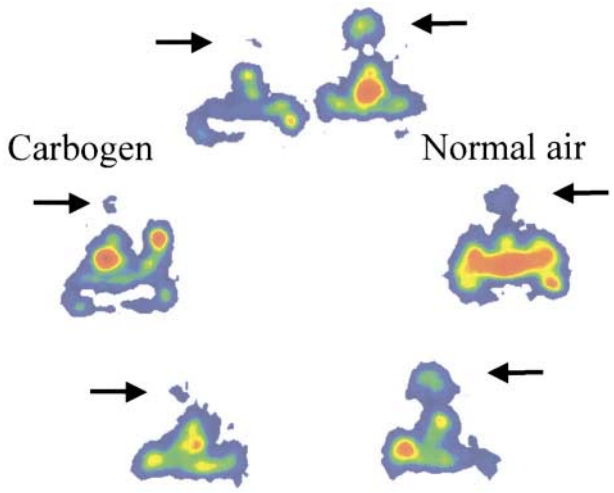

Fig. 1. Transaxial PET image of 6 mice 285 min after [^{18}F]FMISO injection. The 3 mice to the left are breathing carbogen (95% oxygen) and the 3 mice to the right are breathing normal air (21% oxygen). Tumour volumes 400–700 mm^3. Arrows indicate tumours.

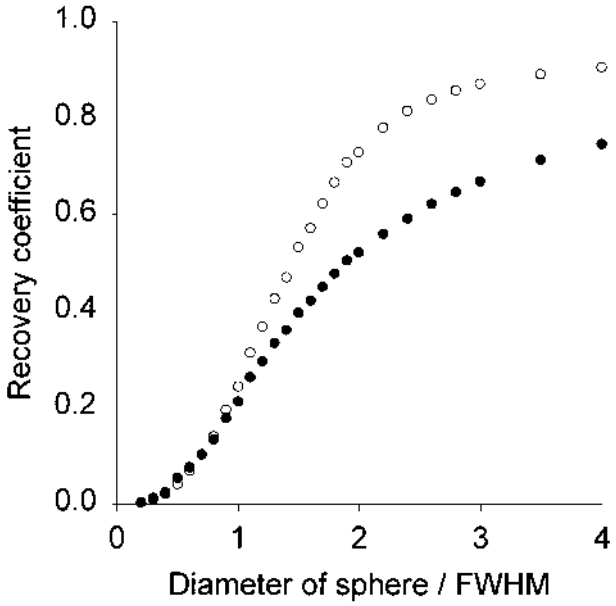

Fig. 2. Simulated recovery coefficients of perfect spheres as a function of sphere diameter divided by the image resolution (FWHM) for ROI methods 1_{ana} (filled symbols) and 2_{act} (open symbols).

RESULTS

Image analysis

Visual analysis of the data was performed in images of transaxial slices reflecting the mean radioactivity concentration over the time from 0 to 5 h after injection. In the FMISO experiments, the heads, brains and the hearts could be identified in the cranial slices (not shown); the tumours were identified on top of the backs of the animals in the intermediate slices; here the bladders of the animals were also seen (see Fig. 1). The tails of the animals were seen in the caudal slices. In the FDG examinations it was not possible to discriminate the hearts of the animals, whereas heads, bladders and tumours were easily defined.

Regions of interest in the tumours

Due to limited resolution of the PET-scanner, the radioactivity concentrations in small objects seem lower than they really are—a phenomenon known as the partial volume effect. The factor by which the radioactivity is reduced is called a 'recovery coefficient'. To account for the partial volume effect, recovery coefficients were calculated for spheres of various diameters, as shown in Fig. 2. This simple estimate is based on synthetic images, representing perfect and homogeneous spheres of unity intensity on a zero background. PET-imaging of these perfect spheres was simulated by convolving the synthetic images with the

measured resolution (point spread function) of the PET scanner, which for simplicity was approximated by a Gaussian function with the same full width half maximum (FWHM) as the measured resolution. In the resulting images, the recovery coefficients were calculated as the mean intensity inside circular regions of interest (ROIs) centred on the spheres. In the measured PET images, the tumours were easily identified in the last part of the scanning procedure (285–295 min after injection for FMISO and 225–295 min after injection for FDG). An ROI was defined in each tumour to measure the amount of tracer bound to the tumour. Two different methods of identifying ROIs were examined:

Method 1. ROI_{ana} (based on anatomical tumour size). The diameters of the tumours and overlying skin were measured with calipers before the scanning procedures. To define an ROI, we used the diameters in the transaxial plane D2 and D3, with a reduction of 2 mm in each diameter to ensure that skin was not included in the ROI used for the PET analysis. An ROI for each tumour was drawn in a transaxial slice in the last time frame of the experiment (285–295 min) by identifying the pixels in the tumour with the highest radioactivity concentration and then drawing an ROI using a circle/ellipse contour with the diameters just mentioned. The average radioactivity concentration in each ROI was corrected by the recovery coefficients in Fig. 2, using a sphere diameter calculated as the average of the two diameters of the ROI. Time activity curves for each tumour ROI were reported as the corrected average radioactivity concentration (Bq/ml tissue) for each time frame (see Fig. 3, panel A).

Method 2. ROI_{act} (based on the radioactivity concentration in tumour). The ROI for each tumour was defined in a transaxial slice by identifying the pixel with the maximum radioactivity concentration and including pixels with activities equal to or higher than 75% of this maximum value (using 75% isocontour tool with ECAT software, carefully avoiding additional tissue). This definition of an ROI results in pixels with at least 75% of maximum radioactivity concentration at the edge of the tumour ROI, but does not rule out the possibility of having pixels with lower activity included between the centre and edge of the ROI. This will be particularly the case if the tumour is very inhomogeneous with respect to uptake of tracer. The ROIs' length and width were measured with the ECAT7 software and a sphere diameter calculated as the mean. To account for the partial volume effect, the mean activity was corrected by computed recovery coefficients as described above. Time activity curves for each tumour ROI was reported as described above.

Reference tissue. In this study we also sought to determine the amount of tracer bound to the tumour tissue in comparison with the activities in reference tissue. Usually this is done by means of radioactivity concentration measurements in blood samples, but this was not possible because of the small blood volume of the mice. We therefore used a reference tissue selected elsewhere in the animals. For the FMISO studies, the reference tissue was selected cranially to the heart level in order to avoid the liver, kidney and bladder, since these organs contribute to the elimination of the tracer. It was possible to identify the hearts of the animals in the first time frame (0–10 min) and the reference tissue was chosen five slices (15.5 mm) cranially to this level. This reference tissue includes muscle, connective tissue, bone, blood and perhaps brain, depending on the exact position of the animal.

The ROI for each reference was defined in a transaxial slice by identifying the pixel with the maximum activity and with the borders defined by an isocontour which enclosed pixels having at least 75% of the maximum activity as described in method 2. The ROI's x and y diameters were measured using the software. The activity of this ROI was reported for the dynamic study characterized by an average radioactivity concentration (Bq/ml tissue) for each time frame (see Fig. 3, panel A). To account for the partial volume effect, recovery coefficients for a sphere were calculated. ROI was approximated to a circle with a diameter calculated as $d = (x + y)/2$ and the mean activity for the ROIs was corrected by this value.

In the FDG studies, large amounts of tracer were bound in the head region of the animals, probably because of FDG-6-phosphate accumulation in the brain. The reference tissue was selected in the abdomen of the animals, 5 slices (15.5 mm) cranially to the tumour level. This reference tissue therefore included muscle, connective tissue, blood, intestines and perhaps kidney and liver tissue as well. The radioactivity concentrations in this reference tissue were particularly heterogeneous, which resulted in ROIs with varying geometric shapes when using the isocontour as the tool for ROI definition. Approximation of the ROI to a circle was thus not possible and using the model for partial volume effect correction as described above was impossible. We defined the reference tissue ROIs as circles with fixed diameters of 15 mm (slightly less than the diameter of a mouse abdomen) (see Fig. 3, panel C). Otherwise, the reference tissue radioactivity was reported and corrected for the partial volume effect, as described above.

In the reference tissue, there was an initial high activity for both tracers followed by a decrease towards a quasi-steady-state with FDG eliminated more rapidly than FMISO. For FDG, a 'steady-state' level was reached approximately 100 min after tracer injection. It is not possible directly to compare the tracers in reference tissue, as the tissue itself was not the same, (see Fig. 3, panels A and C).

In the FMISO studies 5 experimental series including a total of 30 animals were examined; 16 animals breathed carbogen gas and 14 animals were controls. Each single experiment was performed with half of the animals breath-

ing normal air and half of them breathing carbogen. The time activity curves (TACs) of the tumours for ROI methods 1 and 2 showed an initial increase in activity to a peak around 100–120 min after the injection, followed by a slow decrease. This is illustrated in Fig. 3, panel A, for one example. In two mice, the tumours could not be identified by the visual PET image analysis; they were both treated with carbogen and both animals had been given the tracer, since they could be visually identified on the images. In another two mice the tumour activity could not be corrected for partial volume effect, owing to a very small diameter of the ROI. This left 26 tumours for further analysis. In the FDG studies, 3 experimental series including a total of 17 animals were examined; 8 animals were treated with carbogen and 9 animals were breathing air. An example of TACs for a tumour using both methods 1 and 2 is presented in Fig. 3, panel C. The TACs showed an initial increase in radioactivity, peaking at around 40 min after the injection, followed by a slow decrease in activity. For both FMISO and FDG, ROI method 1 using the anatomical sizes of the tumours resulted in higher radioactivity concentrations than those with method 2, based on

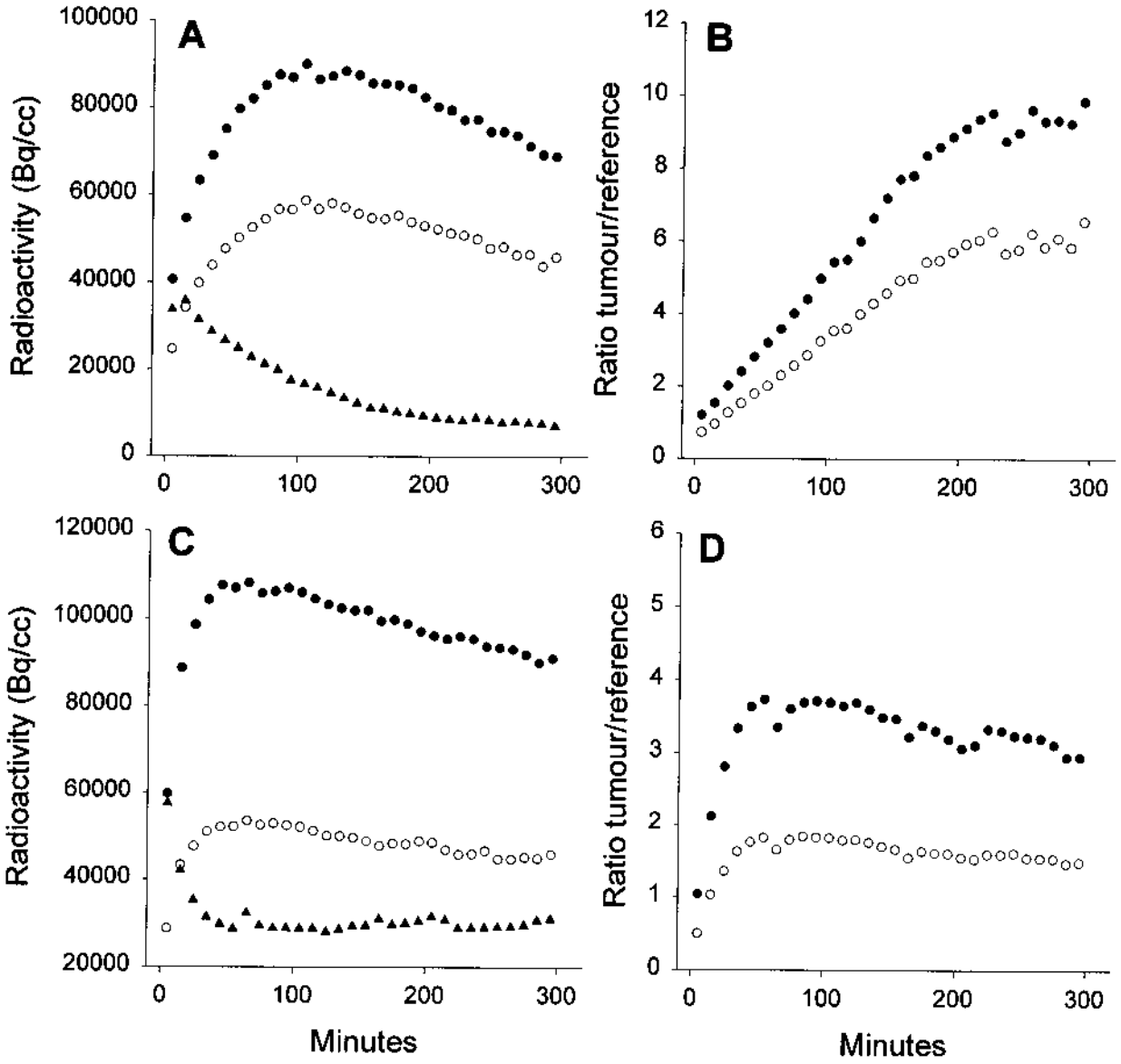

Fig. 3. Panel A: FMISO time activity curves (circles) for a tumour from an air breathing mouse for ROI methods 1_{ana} (filled symbols) and 2_{act} (open symbols). Reference tissue time activity curve for an air breathing mouse (filled triangles). Panel B: Ratio tumour/reference tissue for ROI methods 1_{ana} (filled symbols) and 2_{act} (open symbols). Panel C: FDG time activity curves (circles) for a tumour from an air-breathing mouse for ROI methods 1_{ana} (filled symbols) and 2_{act} (open symbols). Reference tissue time activity curve for an air-breathing mouse (filled triangles). Panel D: Ratio tumour/reference tissue for ROI methods 1_{ana} (filled symbols) and 2_{act} (open symbols).

Table 1

FMISO experiments. Steady-state ratio of tumour to reference radioactivity concentrations

	Normal air with 21% oxygen (13 mice)	Carbogen with 95% oxygen (13 mice)
Method 1 (anatomical defined ROI)		
Median ratio (range)	9.3 (6.4–13.8)	3.3 (0.9–6.4)*
Method 2 (radioactivity defined ROI)		
Median ratio (range)	7.0 (2.9–11.8)	2.3 (0.7–5.1)*
Mean tumour volume μl (range)	581 (311–791)	618 (403–791)[1]

* $p < 0.01$, Mann-Whitney U test, Ratio compared for normal air and carbogen.
[1] NS, T-test, volume compared for normal air and carbogen.

the radioactivity maximum, but in this example the TACs were very similar for both methods.

Tumour to reference tissue ratios

The time course of the ratio between the tumour and reference tissue radioactivities is illustrated in Fig. 3, panels B and D. For FMISO the ratio increased until about 200 min after the tracer injection, after which a steady-state level was reached. For FDG the ratio increased more rapidly with a maximum approximately 60 min after tracer injection, after which it decreased slowly, reaching a quasi-steady-state after 200 min. In Tables 1 and 2 tumour to reference tissue steady-state mean ratios of the radioactivity concentrations (225–300 min after injection) are reported for animals treated with carbogen and animals breathing normal air. We found a significantly higher FMISO ratio in animals breathing air than in animals breathing carbogen. When the tumour TAC for an animal

Table 2

FDG experiments. Steady-state ratio of tumour to reference radioactivity concentrations

	Normal air with 21% oxygen (9 mice)	Carbogen with 95% oxygen (8 mice)
Method 1 (anatomical defined ROI)		
Median ratio (range)	2.7 (1.9–4.7)	2.1 (1.7–2.9)*
Method 2 (radioactivity defined ROI)		
Median ratio (range)	1.5 (1.4–3.5)	1.3 (0.9–2.2)**
Mean tumour volume μl (range)	536 (330–792)	474 (330–748)[1]

* $p = 0.06$, ** $p = 0.01$, Mann-Whitney U test.
[1] NS, T-test, volume compared for normal air and carbogen.

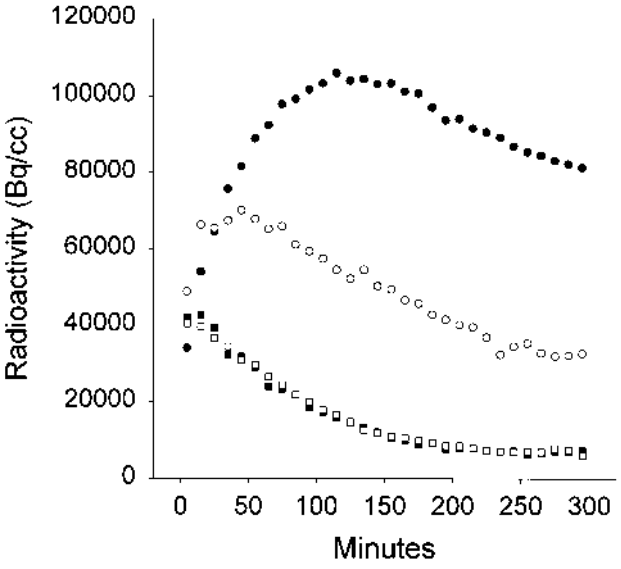

Fig. 4. Time activity curves for two tumours treated with either carbogen (open symbols) or normal air (filled symbols) and for their reference tissue (filled symbols for normal air and open symbols for carbogen). Tumour sizes were comparable, ROI method 1_{ana}.

breathing carbogen was compared with a size-matched tumour TAC from an animal breathing air in that same experiment, we found that the tumour radioactivity in the carbogen-treated animal was lower than that in the air-breathing animal, (see Fig. 4), whereas the reference tissue radioactivities for the differently treated animals were comparable (see Fig. 4). This indicates that the tumour labelling by the hypoxic marker changed with oxygenation status, whereas the reference tissue labelling did not. For FDG we found a significantly higher FDG ratio in animals breathing air compared to those breathing carbogen, when we used method 2, whereas method 1 did not result in significant difference. If TACs for carbogen- and air-breathing mice were compared (data not shown), there was no significant difference in reference tissue radioactivity, indicating that the uptake of FDG did not change with the degree of oxygen content in the blood of the animals. In fact, the oxygenation status of all the PET examined tumours was also measured with an Eppendorf Histograph and the oxygen partial pressure (pO_2) distributions under the control and carbogen breathing conditions determined. It was found that the median value of tumour pO_2 less than or equal to 2.5 mmHg was 35% in the control animals and 15% in those animals that breathed carbogen, and this difference was significant (Mann-Whitney U test, $p < 0.05$).

DISCUSSION

In our study we examined the possibility of labelling experimental tumours with [^{18}F]fluorinated compounds.

The experimental set-up which allowed simultaneous examination of six animals gave us an opportunity to compare experimental modification of the oxygen supply. In PET studies the identification of a tumour depends solely on the amount of radioactivity in that tumour, because of metabolic activity and not on account of any morphological characteristics. In our study, the tumours were well demarcated because they were situated subcutaneously on the backs of the mice. This position made it possible to measure the tumours and using these measurements give estimations of tumour areas in the transaxial plane. As a result, we were able to examine two models for identifying ROIs. Both models were feasible for both tracers, but further validation was carried out for FMISO only. The ratios are presented in Tables 1 and 2 and Fig. 5. For the majority of the tumours, ROI method 1, where the measured sizes of the tumours were used for defining the ROIs, gave the largest ratios, but the ratios calculated with both methods were closely correlated (see Fig. 5). Ideally, the ratios should be identical, when the correction for partial volume is made. However, as stated in the Methods section of this paper, the recovery coefficients calculated to account for the partial volume effect are based on homogeneous spheres, which is not always the case here, since the uptake of the tracer is heterogeneous. Furthermore, the measurement of the tumour diameters, and especially the reduction of diameters to avoid skin inclusion, might result in errors in the ROI definition. Defining tumour contour by radioactivity alone can result in overestimation of tumour sizes. This issue must be borne in mind in clinical studies where an additional CT or MRI examination can provide additional information concerning the morphology of a tumour. With both methods we ended up with an average radioactivity for a given area, and heterogeneity in the distribution of the tracer was not reflected in the endpoint. However, in this experimental study where the ROIs are small compared to the resolution, it serves no purpose to pursue this issue. For clinical purposes, it is important to reflect heterogeneity, as this might give a truer report of hypoxic areas, and for larger tumour volumes it should be possible to conduct pixel to pixel analyses.

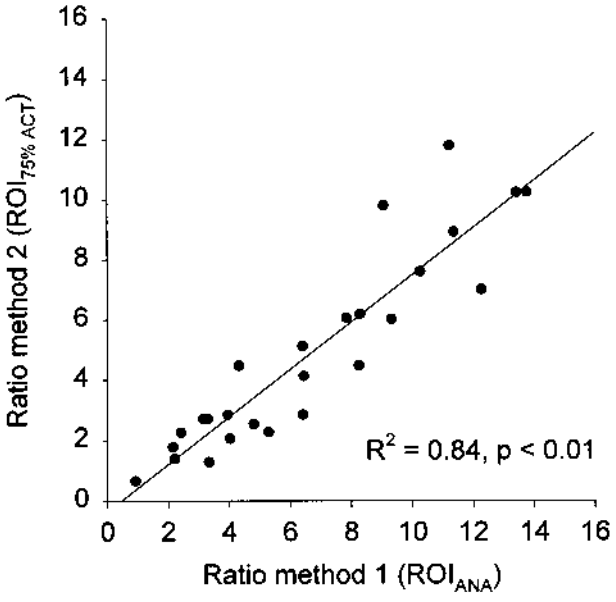

Fig. 5. Comparison of the FMISO ratios obtained by ROI methods 1 and 2. Solid line shows correlation between methods 1 and 2.

In the carbogen series, two of the tumours examined could not be identified by the visual PET analysis. The labelling was simply too low. This implies that the number of hypoxic cells in these particular tumours must have been very low. For clinical purposes this poses an interesting question. It means that if a patient with a well-oxygenated tumour is examined by this tracer, it can be troublesome even to locate the tumour, as few or even no hot spots may be found in the PET image. In the study by Koh et al. (16), 2 out of 8 human tumours did not show pixels above a selected threshold for the tumour to plasma ratio of [^{18}F]FMISO. However, in that particular study the patients also underwent CT scanning, so location of the tumour could be determined.

As an endpoint for reporting the PET data, we used the ratio between radioactivity in the tumour and reference tissue. A reference tissue which consisted of muscle tissue alone, as suggested by Chapman et al. (13), was not possible for these animal studies because of the small size of the mice. Instead, for the FMISO studies we had a well-defined area where none of the internal organs involved in tracer elimination were included. The time activity curves for this reference tissue showed slow elimination patterns. This endpoint would also be suitable for clinical examinations and here it would be possible to select pure muscle tissue, as the volumes obviously would be larger. The timing for evaluating accumulation of radioactive tracers in tissues is always a compromise between the physiological half-lives of the tracers and the distribution in the tissues, which is dependent on metabolism and excretion of tracer and the uptake of tracer in the specific tissues. In this FMISO study with the relative slow excretion of tracer from the reference tissue, the difference between normal tissue and tumour increased throughout almost the whole study, reaching a quasi-steady-state after about 225 min. This is in good agreement with a study by Kubota et al. (25), where [^{18}F]FMISO given to tumour-bearing rats was distributed likewise. In the clinical study by Koh et al. (16) the 2-h post injection tumour/plasma ratio was found most informative and also acceptable for the patients involved.

The compound FMISO has been shown to label hypoxic cells in vitro (26, 27) and in tumours in previous preliminary clinical studies (16, 17, 28). In our tumour model,

hypoxia has been shown to exist (24, 29, 30) and it has previous been demonstrated that this hypoxia can be diminished if the animals breathe carbogen (30). Here we have shown that FMISO labels these tumours and that the tumour labelling is significantly less in mice that are given carbogen. Since the carbogen- and normal air-treated tumours were otherwise comparable, this difference in tracer labelling is consistent with labelling of hypoxia.

The aim of this study was not to define a specific amount of tracer accumulation as indicative of hypoxia. This is possible if PET measurements are done in combination with invasive procedures to measure oxygen content, for instance pO_2 electrode measurements or if the labelling is compared with the hypoxic fraction measured with the paired survival curve assay. Rasey et al. (31) did a comparison between the biodistribution of fluoromisomidazole in mouse tumours and blood and estimated hypoxic fractions for tumours of comparable size, and they concluded that FMISO tumour blood ratios might be predictive for hypoxic fraction. However, in a recent study by the group it was shown that the FMISO-derived radiobiologically hypoxic fraction in tumours in rats breathing 10% oxygen was much lower than the hypoxic fraction derived by radiation response data (32), and it was argued that invasive oxygen measurements are needed.

For the FDG studies, we had problems defining a reference tissue, and the abdominal transaxial slice that was used includes internal organs. Time activity curves for this tissue showed rapid exponential elimination patterns but with a generally lower decrease than with [^{18}F]FMISO (see Fig. 3). When the ratios for FMISO and FDG are compared, FDG gives lower ratios and this could partly be explained by the mentioned lower decrease with time in the reference tissue. A direct comparison between the ratios will thus not be possible, because of the different reference tissues. This, however, does not explain why we were able to find a significant difference was found between FDG uptake in carbogen-treated tumours and normal air-treated tumours only by the ROI method 2, whereas method 1 based on the anatomical measurements showed no significance. In the study by Minn et al. (19) it was shown that FDG accumulates more in hypoxic than in normoxic cells. However in the recent work by Kubota et al. (25), where uptake of [^{18}F]FMISO, FDG and methionine (Met) in rat tumours was examined by autoradiography, they showed that the uptake of FMISO and FDG is not uniform morphologically. FMISO tended to accumulate in areas near necrosis while FDG accumulated with a more uniform distribution throughout the tumours. Furthermore, they showed that hypoxic tumours have significantly higher uptake of FMISO than non-hypoxic tumours, and that FDG uptake was lower in hypoxic tumours compared to controls. As argued above, discussing heterogeneity in radioactive labelling makes less sense in these small tumours so this study does not provide any data on the FDG versus FMISO labelling. However, the C3H mammary tumour used in our study could have a more restricted uptake of glucose compared with that in other tumour models or human tumours. For future experimental studies using FDG, other tumour lines should be tested.

CONCLUSION

In this study we found that [^{18}F]FMISO labels experimental tumours and that it is feasible to detect this labelling with PET. With modification of oxygen content in the blood the labelling with [^{18}F]FMISO was significantly changed, which implies that the tracer labelled the hypoxic cells. A tumour to reference tissue ratio was defined, which was used for evaluation of tracer accumulation in these small tumours. In this animal study, tracer accumulation in the tissues was best evaluated between 3.5 and 5 h after injection. For future experiments, we suggest further comparative measurements between PET examinations and pO_2 measurements should be carried out to quantify the hypoxia measured by the PET methodology. FDG was able to label the experimental tumours in this study, but it was only possible to use this marker to discriminate the levels of tumour hypoxia in control and carbogen-breathing animals by the use of one of the evaluated methods. This suggests that additional studies are required before this agent can be considered as a potential marker for hypoxia, at least in our tumour model.

ACKNOWLEDGEMENTS

The authors thank I. M. Johansen, D. Grand and M. H. Simonsen for excellent technical assistance. The study was supported by a grant from The Danish Cancer Society.

REFERENCES

1. Moulder JE, Rockwell S. Hypoxic fractions of solid tumors: experimental techniques, methods of analysis, and a survey of existing data. Int J Radiat Oncol Biol Phys 1984; 10: 695–712.
2. Grau C, Horsman MR, Overgaard J. Improving the radiation response in a C3H mouse mammary carcinoma by normobaric oxygen or carbogen breathing. Int J Radiat Oncol Biol Phys 1992; 22: 415–9.
3. Grau C, Horsman MR, Overgaard J. Influence of carboxyhemoglobin level on tumor growth, blood flow, and radiation response in an experimental model. Int J Radiat Oncol Biol Phys 1992; 22: 421–4.
4. Overgaard J, Horsman MR. Modification of hypoxia-induced radioresistance in tumors by the use of oxygen and sensitizers. Sem Radiat Oncol 1996; 6: 10–21.
5. Sutherland RM, Ausserer WA, Murphy BJ, Laderoute KR. Tumour hypoxia and heterogeneity: Challenges and opportunities for the future. Sem Radiat Oncol 1996; 6: 59–70.
6. Giaccia AJ. Hypoxic stress proteins: survival of the fittest. Sem Radiat Oncol 1996; 6: 46–58.
7. Graeber TG, Osmanian C, Jacks T, et al. Hypoxia-mediated selection of cells with diminished apoptotic potential in solid tumours. Nature 1996; 379: 88–91.

8. Dachs GU, Chaplin DJ. Microenvironmental control of gene expression: implications for tumor angiogenesis, progression, and metastasis. Sem Radiat Oncol 1998; 8: 208–16.
9. Kolstad P. Intercapillary distance, oxygen tension and local recurrence in cervix cancer. Scand J Clin Lab. Invest 1968; (Suppl 106): 145–57.
10. Nordsmark M, Overgaard M, Overgaard J. Pretreatment oxygenation predicts radiation response in advanced squamous cell carcinoma of the head and neck. Radiother Oncol 1996; 41: 31–9.
11. Hockel M, Schlenger K, Aral B, Mitze M, Schaffer U, Vaupel P. Association between tumor hypoxia and malignant progression in advanced cancer of the uterine cervix. Cancer Res 1996; 56: 4509–15.
12. Brizel DM, Scully SP, Harrelson JM, et al. Tumor oxygenation predicts for the likelihood of distant metastases in human soft tissue sarcoma. Cancer Res 1996; 56: 941–3.
13. Chapman JD, Engelhardt EL, Stobbe CC, Schneider RF, Hanks GE. Measuring hypoxia and predicting tumor radioresistance with nuclear medicine assays. Radiother Oncol 1998; 46: 229–37.
14. Chapman JD, Franko AJ, Sharplin J. A marker for hypoxic cells in tumours with potential clinical applicability. Br J Cancer 1981; 43: 546–50.
15. Grunbaum Z, Freauff SJ, Krohn KA, Wilbur DS, Magee S, Rasey JS. Synthesis and characterization of congeners of misonidazole for imaging hypoxia. J Nucl Med 1987; 28: 68–75.
16. Koh WJ, Rasey JS, Evans ML, et al. Imaging of hypoxia in human tumors with [F-18]fluoromisonidazole. Int J Radiat Oncol Biol Phys 1992; 22: 199–212.
17. Rasey JS, Koh WJ, Evans ML, et al. Quantifying regional hypoxia in human tumors with positron emission tomography of [^{18}F]fluoromisonidazole: a pretherapy study of 37 patients. Int J Radiat Oncol Biol Phys 1996; 36: 417–28.
18. Clavo AC, Brown RS, Wahl RL. Fluorodeoxyglucose uptake in human cancer cell lines is increased by hypoxia. J Nucl Med 1995; 36: 1625–32.
19. Minn H, Clavo AC, Wahl RL. Influence of hypoxia on tracer accumulation in squamous-cell carcinoma: in vitro evaluation for PET imaging. Nucl Med Biol 1996; 23: 941–6.
20. Lim JL, Berridge MS. An efficient radiosynthesis of [^{18}F]fluoromisonidazole. Appl Radiat Isot 1993; 44: 1085–91.
21. Toorongian SA, Mulholland GK, Jewett DM, Bachelor MA, Kilbourn MR. Routine production of 2-deoxy-2-[^{18}F]fluoro-D-glucose by direct nucleophilic exchange on a quaternary 4-aminopyridinium resin. Int J Rad Appl Instrum.[B]. 1990; 17: 273–9.
22. Overgaard J. Simultaneous and sequential hyperthermia and radiation treatment of an experimental tumor and its surrounding normal tissue in vivo. Int J Radiat Oncol Biol Phys 1980; 6: 1507–17.
23. Horsman MR, Khalil AA, Siemann DW, et al. Relationship between radiobiological hypoxia in tumors and electrode measurements of tumor oxygenation. Int J Radiat Oncol Biol Phys 1994; 29: 439–42.
24. Olive PL, Horsman MR, Grau C, Overgaard J. Detection of hypoxic cells in a C_3H mouse mammary carcinoma using the comet assay. Br J Cancer 1997; 76: 694–9.
25. Kubota K, Tada M, Yamada S, et al. Comparison of the distribution of fluorine-18 fluoromisonidazole, deoxyglucose and methionine in tumour tissue. Eur J Nucl Med. 1999; 26: 750–7.
26. Rasey JS, Grunbaum Z, Magee S, et al. Characterization of radiolabeled fluoromisonidazole as a probe for hypoxic cells. Radiat Res 1987; 111: 292–304.
27. Rasey JS, Nelson NJ, Chin L, Evans ML, Grunbaum Z. Characteristics of the binding of labeled fluoromisonidazole in cells in vitro. Radiat Res 1990; 122: 301–8.
28. Koh WJ, Bergman KS, Rasey JS, et al. Evaluation of oxygenation status during fractionated radiotherapy in human nonsmall cell lung cancers using [^{18}F]fluoromisonidazole positron emission tomography. Int J Radiat Oncol Biol Phys. 1995; 33: 391–8.
29. Horsman MR, Khalil AA, Nordsmark M, Grau C, Overgaard J. Measurement of pO_2 in a murine tumour and its correlation with hypoxic fraction. Adv Exp Med Biol 1994; 345: 493–500.
30. Horsman MR, Nordsmark M, Khalil AA, et al. Reducing acute and chronic hypoxia in tumours by combining nicotinamide with carbogen breathing. Acta Oncol 1994; 33: 371–6.
31. Rasey JS, Koh WJ, Grierson JR, Grunbaum Z, Krohn KA. Radiolabelled fluoromisonidazole as an imaging agent for tumor hypoxia. Int J Radiat Oncol Biol Phys 1989; 17: 985–91.
32. Rasey JS, Casciari JJ, Hofstrand PD, Muzi M, Graham MM, Chin LK. Determining hypoxic fraction in a rat glioma by uptake of radiolabeled fluoromisonidazole. Radiat Res 2000; 153: 84–92.